Volume 3 | Number 10 | October 2016

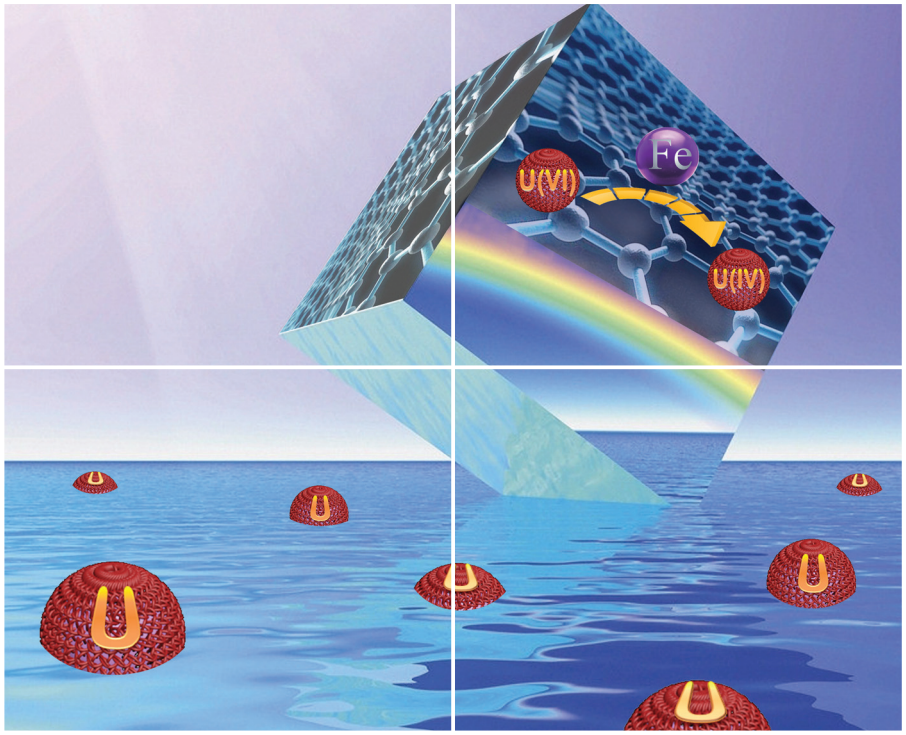

INORGANIC CHEMISTRY

FRONTIERS

Chinese Chemical Society
PEKING UNIVERSITY 1898
ROYAL SOCIETY OF CHEMISTRY

http://rsc.li/frontiers-inorganic

INORGANIC CHEMISTRY
FRONTIERS

RESEARCH ARTICLE

Cite this: *Inorg. Chem. Front.*, 2016, **3**, 1289

Revisiting $Ce_3Pt_4Ge_6$ – crystal structure and physical properties†

Oliver Janka,*[a,b] Rolf-Dieter Hoffmann,[b] Matthias Eilers-Rethwisch,[b] Ute Ch. Rodewald,[b] Oliver Niehaus[b,c] and Rainer Pöttgen[b]

Received 14th July 2016,
Accepted 17th August 2016

DOI: 10.1039/c6qi00248j

rsc.li/frontiers-inorganic

Structural reinvestigations of $Ce_3Pt_4Ge_6$ on high quality single crystals revealed additional reflections contradicting the previously reported structure featuring half occupied crystallographic sites for this compound. The structure could be solved and refined in the orthorhombic (3 + 1)D superspace group $Cmcm(\alpha,0,0)0s0$ with $\alpha = 0.5a^*$ and lattice parameters of a = 441.17(2), b = 2618.26(14) and c = 441.33(2) pm using the super space approach. The description of the modulated structure as commensurate case allows for an ordering of the Ce2/Ge3 atoms and the respective voids caused by the 50% occupation. The corresponding approximant can be described in the orthorhombic crystal system with space group *Pnma* and lattice parameters of a = 2618.26(14), b = 441.33(2) and c = 882.34(2) pm. Investigations of the magnetic properties revealed a magnetic moment of μ_{eff} = 2.48(1)μ_B/Ce atom and a Weiss constant of θ_p = −39(5) K, indicating stable trivalent cerium. No clear magnetic ordering was evident from the susceptibility measurements. Heat capacity investigations showed a λ-shaped anomaly at T = 2.1(1) K. Resistivity measurements show values corresponding to $Ce_3Pt_4Ge_6$ being a metal, however nearly temperature independent behavior is observed down to low temperatures. A shallow minimum and an abrupt drop suggest the title compound to be a Kondo material.

Introduction

The isothermal section of the Ce–Pt–Ge phase diagram at 873 K has carefully been studied by Gribanov *et al.*[1] The phase analytical work, based on X-ray powder and single crystal diffraction as well as metallography in combination with electron microscopy revealed 12 ternary germanides. Most of the structures of these phases have been solved and preliminary physical property studies have been performed.[2–23] To give some examples, CePtGe[9,19] and $CePt_2Ge_2$[10] order antiferromagnetically at T_N = 4 and 2.2 K, respectively. $CePt_5Ge_3$ is a low-dimensional magnetic material with an ordering temperature of 1.1 K.[21]

In the original work, the structures of CePtGe[3] and $Ce_3Pt_4Ge_6$[11] were reported with mixed and partially occupied sites, respectively. Reinvestigation of the CePtGe structure[18,19] revealed weak superstructure reflections, originating from platinum–germanium ordering. The single crystal data clearly stated the orthorhombic YPdSi structure type. The $Ce_3Pt_4Ge_6$ structure[11] was refined in space group *Bmmb* (non-standard setting of *Cmcm*) with half-occupied Ce2 (4*c*) and Ge3 (8*g*) sites. Similar composition, but different space group symmetry was observed for the $RE_3Pt_4Ge_6$ representatives with the smaller rare earth (RE) elements.[24–26] The $Y_3Pt_4Ge_6$ structure[24] as well as the silicide $Yb_{\sim 3}Pt_{\sim 4}Si_{6-x}$ (x = 0.3)[26] were described in the monoclinic space group $P2_1/m$ and the germanides $RE_3Pt_4Ge_6$ (RE = Pr, Nd, Sm, Gd, Tb, Dy)[25] were reported with space group *Pnma* which allows for an ordering of all atomic sites. Reinvestigation of the $Ce_3Pt_4Ge_6$ structure by these authors gave hints for cerium–germanium ordering. Single crystals taken from a long-term annealed sample showed diffuse intensities.

We became interested in these order–disorder problems when solving the structure of a new monoclinic cerium–gold–germanide with an approximate composition $Ce_3Au_{\sim 5.5}Ge_{\sim 4.5}$[27] and presumably $Y_3Pt_4Ge_6$ structure. In the course of these systematic investigations we also synthesized new $Ce_3Pt_4Ge_6$ samples and obtained well shaped single crystals upon annealing arc-melted precursors in a water-cooled sample chamber of an induction furnace. Herein we report on crystal chemical data on the ordered phase and the magnetic properties of $Ce_3Pt_4Ge_6$. The order–disorder difficulty is discussed on the basis of a group–subgroup scheme.

[a]*Institut für Chemie, Carl von Ossietzky Universität, Carl-von-Ossietzky Strasse 9-11, D-26129 Oldenburg, Germany. E-mail: ocjanka@uni-muenster.de*
[b]*Institut für Anorganische und Analytische Chemie, Universität Münster, Corrensstraße 30, D-48149 Münster, Germany*
[c]*NRW Graduate School of Chemistry, Universität Münster, Corrensstraße 30, D-48149 Münster, Germany*

†Dedicated to Professor Mercouri G. Kanatzidis on the occasion of his 60th birthday.

Experimental

Synthesis

$Ce_3Pt_4Ge_6$ was synthesized from the elements using cerium ingots (Sigma-Aldrich), platinum sheets (Agosi AG), and germanium lumps (Chempur), all with stated purities better than 99.9%. Pieces of cerium were first arc-melted under an argon pressure of 800 mbar in a water cooled copper heart.[28] All starting materials were weighed in the ideal 3 : 4 : 6 ratio (Ce : Pt : Ge) and arc-melted under an argon pressure of 800 mbar. The obtained button was remelted and turned over several times to increase the homogeneity. In a subsequent step the ingot was heated to temperatures just below the melting point for 2 h in a high frequency furnace (Hüttinger Elektronik, Freiburg, Germany, Typ TIG 2.5/300).[29] Afterwards the sample was slowly cooled to room temperature. The sample shows metallic luster and is stable in air over months.

X-ray diffraction

The polycrystalline sample was characterized by a Guinier pattern (imaging plate detector, Fujifilm BAS-1800 scanner) with CuKα_1 radiation using α-quartz (a = 491.30, c = 540.46 pm, Riedel-de-Häen) as an internal standard.

Correct indexing of the diffraction lines was ensured through an intensity calculation. The lattice parameters were obtained through least-squares fits[30] with standard deviations smaller than ±0.1 pm for all axes.

Irregularly shaped crystals of $Ce_3Pt_4Ge_6$ were obtained by mechanical fragmentation of the annealed arc-melted button. These fragments were glued to thin quartz fibers using beeswax. The crystal quality was tested by Laue photographs on a Buerger camera (white molybdenum radiation, image plate technique, Fuji film, BAS-1800). Intensity data sets of a suitable crystal were collected at room temperature by use of a Stoe IPDS II diffractometer (graphite-monochromatized MoK$_\alpha$ radiation; oscillation mode). Numerical absorption correction was applied to the data set. All relevant crystallographic data and details of the data collections and evaluations are listed in Table 1.

Further details on the structure refinement are available from Fachinformationszentrum Karlsruhe, D-76344 Eggenstein-Leopoldshafen (Germany), E-mail: crysdata@fiz-karlsruhe.de, by quoting the Registry no. CSD 431566.

Physical property investigations

Magnetism. A polycrystalline piece of the annealed ingot was packed in kapton foil and attached to the sample holder rod of a Vibrating Sample Magnetometer (VSM) unit for measuring the magnetization M(T,H) in a Quantum Design Physical–Property–Measurement–System (PPMS). The sample was investigated in the temperature range of 2.0–300 K with magnetic flux densities up to 80 kOe.

Heat capacity. For the heat capacity measurements, one piece of the sample was fixed to a pre-calibrated heat capacity puck using Apiezon N grease and investigated in the temperature range of 1.9–300 K.

Electrical resistivity. An annealed button was embedded in a polymethyl-methacrylate (PMMA) matrix and after solidification of the polymer polished on one side until a cross section of at least 3 × 3 mm^2 was visible. The sample was subsequently removed from the polymer by dissolving the matrix in acetone. In a second step the ingot was embedded again in PMMA in a self-build mold which allows parallel polishing of the second side. The sample was polished until an approximately 1 mm thick specimen remained inside the polymer matrix. The disc shaped sample was removed by again dissolving the PMMA matrix. The resistivity measurement was carried out in the AC transport mode[32] of a Quantum-Design Physical-Property-Measurement-System (PPMS). The ACT puck was modified by a van-der-Pauw press contact assembly purchased from Wimbush Science & Technology. The probes are spring contacts, gold plated over nickel; the distance between the pins was set to 2 mm. The resistivity was measured between 2–300 K with a data point every 0.1 K up to 10 K and a data point every 2 K up to 300 K. A maximum current of 10 mA was used; the AC frequency was set to 29 Hz with a measurement time of 1 s. The recorded data of channels 1 & 2 was converted according to the van-der-Pauw equation given in the Quantum Design Application Note 1076-304.

Table 1 Crystallographic data and structure refinement for $Ce_3Pt_4Ge_6$

Empirical formula	$Ce_3Pt_4Ge_6$
Superspace group	$Cmcm(\alpha,0,0)0s0$
	$\alpha = 1/2\ a^*$
Molar mass	1636.2 g mol^{-1}
Unit cell dimensions	a = 441.17(2) pm
	b = 2618.26(14) pm
	c = 441.33(2) pm
	V = 0.5098 nm^3
Calculated density	10.66 g cm^{-3}
Linear absorption coeff.	85.0 mm^{-1}
Transm. ratio (min/max)	0.096, 0.190
F(000)	1356
Crystal size/μm	30 × 30 × 35
Diffractometer	IPDS-II
Wavelength	MoKα (71.073 pm)
Detector distance	90 mm
Exposure time	8 min
Integr. param./A, B, EMS	9.9/1.5/0.012
θ range	2.4–30.7 °
Range in $hklm$	±6; ±37; ±6; ±1
Total no. reflections	23224
Independent reflections	1360 (R_{int} = 0.0519)
Reflections with $I \geq 3\sigma(I)$	930 (R_σ = 0.0112)
Main + satellite	930 + 430
Data/parameters	1360/63
Goodness-of-fit	2.07
Final R indices [$I \geq 3\sigma(I)$]	R_M = 0.0186/wR_M = 0.0451
	R_S = 0.0751/wR_S = 0.1480
R indices for all data	R_M = 0.0227/wR_M = 0.0459
	R_S = 0.1243/wR_S = 0.1557
Extinction scheme	Lorentzian isotropic[31]
Extinction coefficient	222(12)
Largest diff. peak and hole/e Å^{-3}	8.71, −3.64

Results and discussion

Structure refinement

The obtained intensity data set of $Ce_3Pt_4Ge_6$ was initially indexed in analogy to the structure solution of $Pr_3Pt_4Ge_6$ in the

orthorhombic space group *Pnma* (no. 62) with lattice parameters of a = 2625.4(8), b = 439.3(1) and c = 884.0(3) pm.[25] However both, the monoclinic unit cell (a = 882.8(2), b = 441.24(8), c = 1325.5(3) pm and β = 99.62(2) °) in analogy to $Y_3Pt_4Ge_6$[24] as well as an orthorhombic *C*-centered cell with space group *Cmcm* (a = 441.9(1), b = 2622.2(5), c = 442.2(1) pm) in analogy to the first report of $Ce_3Pt_4Ge_6$[11] could be found using the automated indexing features. Fig. 1 shows a selected *h*1*l* area of the reconstructed diffraction patterns indicating the cells found in literature as well as our interpretation. A careful investigation of the reconstructed diffraction patterns indicated systematically extinct reflections (red square) needed in order to justify the *P*-centered orthorhombic cell (Fig. 1, left). For the *C*-centered orthorhombic cell (denoted as *Bbmm* here) additional reflections along 1/2 c^* are found in our diffraction experiments making this interpretation as 3D structure obsolete (Fig. 1, right).

Finally the description in the *P*-centered monoclinic cell lacks the interpretation of the additional reflections with 1/4 a^* (green circles) and exhibits systematically absent reflection violations (red squares) for the interpretation as a primitive lattice (Fig. 1, top). A closer look at the reconstructed diffraction patterns reveals two possibilities to index all observed reflections. One possibility is to use the depicted *Bbmm* cell shown in Fig. 1 (right) along with a q-vector q = (0, 0, 1/2 c^*), the other one is to use the depicted monoclinic cell with q = (1/4 a^*, 0, 1/2 c^*). Both possible cell settings have been integrated including all satellite reflections. The structure was subsequently solved by the program package Superflip,[33] included in the Jana2006 package, which was used for the refinement.[34,35] The corresponding superspace groups *Cmcm*(α,0,0)0*s*0 (SSG 63.1.13.2) and *P*2$_1$/*m*(α,0,γ)00 (SSG 11.1.2.1) have been identified. The notation of Stokes, Campbell and van Smaalen for the superspace groups was used.[36,37] Since both refinements gave identical residuals, the higher symmetry was chosen and will be described in the following. The symmetry operations for the orthorhombic superspace group are listed in Table 2.

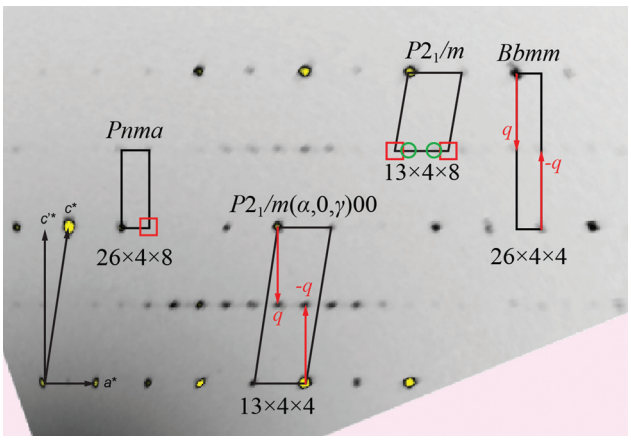

Fig. 1 Sections of the (reconstructed) diffraction pattern of $Ce_3Pt_4Ge_6$. The different unit cells found in the literature are drawn to show the possible (mis)interpretations of the data. Also the monoclinic interpretation in superspace group *P*2$_1$/*m*(α,0,γ)00 with α = 1/4 a^* and γ = 1/2 c^* is shown.

Table 2 Symmetry operations for the orthorhombic (3 + 1)D super space group *Cmcm*(α,0,0)0*s*0

*x*1	*x*2	*x*3	*x*4
−*x*1	−*x*2	*x*3 + 1/2	−*x*4
−*x*1	*x*2	−*x*3 + 1/2	−*x*4 + 1/2
*x*1	−*x*2	−*x*3	*x*4 + 1/2
−*x*1	−*x*2	−*x*3	−*x*4
*x*1	*x*2	−*x*3 + 1/2	*x*4
*x*1	−*x*2	*x*3 + 1/2	*x*4 + 1/2
−*x*1	*x*2	*x*3	−*x*4 + 1/2
*x*1 + 1/2	*x*2 + 1/2	*x*3	*x*4
−*x*1 + 1/2	−*x*2 + 1/2	*x*3 + 1/2	−*x*4
−*x*1 + 1/2	*x*2 + 1/2	−*x*3 + 1/2	−*x*4 + 1/2
*x*1 + 1/2	−*x*2 + 1/2	−*x*3	*x*4 + 1/2
−*x*1 + 1/2	−*x*2 + 1/2	−*x*3	−*x*4
*x*1 + 1/2	*x*2 + 1/2	−*x*3 + 1/2	*x*4
*x*1 + 1/2	−*x*2 + 1/2	*x*3 + 1/2	*x*4 + 1/2
−*x*1 + 1/2	*x*2 + 1/2	*x*3	−*x*4 + 1/2

After refinement of the basic structure the satellites were added to the refinement and positional or occupational modulations for all atoms were applied. In addition, it was possible to refine modulated anisotropic atomic displacement parameters (ADP) for all atoms. The Fourier maps for all atoms showing significant modulations are depicted in Fig. 2. The space group allows for additional degrees of freedom, however some modulation components are very small (Table 3). While Ce1, Pt1, Pt2, Ge1 and Ge2 show positional modulations along *x*1/*x*4 and *x*3/*x*4, Ce2 and Ge3 exhibit occupational modulations along *x*3/*x*4. The occupational modulations were fitted using a crenel function; for the positional modulations simple harmonic functions were used. As a check for the correct composition, the occupancy parameters were refined in a separate series of least-squares cycles. All sites were fully occupied within three standard deviations. There was no indication of mixing on any site. The final difference electron-density synthesis was flat.

Due to the q-vector component α = 1/2 a^*, the crystal structure can be refined as commensurate case in the corresponding orthorhombic superstructure with space group *Pbnm* and a doubled a axis. Standardization finally leads to space group *Pnma* and lattice parameters of a = 2618.26(14), b = 441.33(2) and c = 882.34(2) pm. This unit cell corresponds to the solution of the compounds in the $RE_3Pt_4Ge_6$ (RE = Pr–Dy) series,[25] however in our description all intensities were handled avoiding non-space group specific extinctions.

Crystal chemistry

The building blocks and motifs obtained by the refinement are the same compared to those presented in the previous descriptions in the orthorhombic space groups *Cmcm*,[11] *Pnma*[25] and the monoclinic description of $Y_3Pt_4Ge_6$ in the space group *P*2$_1$/*m*.[24] However one previous work needed half-occupied sites for Ce and Ge atoms in order to describe the structure.[11] The other papers stated either the solution was

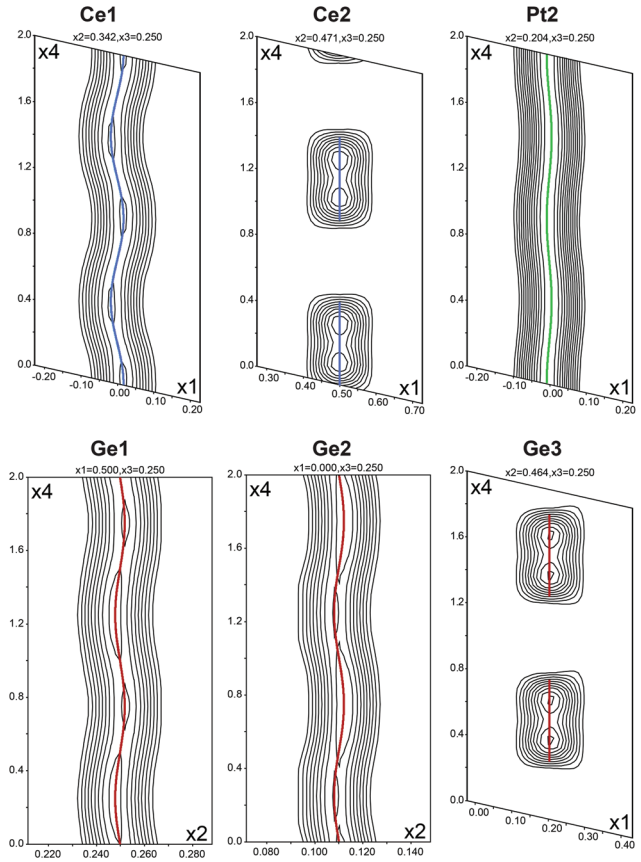

Fig. 2 Sections of the Fourier maps (based on F_{obs}) of the orthorhombic (3 + 1)D refinement with superspace group *Cmcm*(α,0,0)0*s*0 (α = 1/2 *a**) of the commensurately modulated structure of $Ce_3Pt_4Ge_6$. Summation over 100 pm of the projected directions was conducted. Contour lines for all atoms correspond to a difference of 10 e Å^{-3}, each.

achieved by "crystal chemical considerations"[24] or mentioned that the unit cell was chosen under "consideration of the very weak reflections causing a doubling of the *a* axis".[25] These statements suggest that the diffraction patterns might have looked comparable to our investigations (*vide supra*), but were misinterpreted.

Using the motifs highlighted by Venturini *et al.* for $Y_3Pt_4Ge_6$, the structure can be described as an intergrowth between $CaBe_2Ge_2$- and $YIrGe_2$-type slabs. The latter forms pentagonal prisms built by Ir and Ge (here Pt and Ge), which are linked alternatively (up/down) to form layers that are connected further over the pentagonal faces to form a three-dimensional framework. The pentagonal prisms are occupied by the Y^{3+} cations, here Ce2. The $CaBe_2Ge_2$ arrangements consist of tetrahedral [$GeBe_{4/4}$] layers (here Pt and Ge), which are stacked along [100] and exhibit only Ge–Be bonds. The six-membered rings formed by the stacking of the layers are occupied by the Ca^{2+} cations, here Ce1. Due to the occupational modulation of the Ce2 and Ge3 atoms, the pentagonal prisms are allowed to order, facing either to the right or to the left along the *a* axis. In contrast to the description of Gribanov *et al.*, no half occupied sites are needed in this description.

Table 3 Atomic positions, Fourier coefficients of the modulation functions (sin) and equivalent isotropic displacement parameters (pm^2) of $Ce_3Pt_4Ge_6$, superspace group *Cmcm*(α,0,0)0*s*0 with α = 1/2 *a**. All atoms occupy Wyckoff positions 4*c*

Atom	Occ.	Wave	*x*	*y*	*z*	U_{eq}
Ce1	1		0	0.34219(3)	1/4	96(2)
		sin	0.0174(3)	0	0	
		cos	0	0.00002(5)	0	
Ce2	0.5		1/2	0.47112(4)	1/4	94(3)
	$x4_0$ = 0.25	crenel	—	—	—	
Pt1	1		1/2	0.06271(1)	1/4	77(1)
		sin	0.00094(17)	0	0	
		cos	0	−0.00009(3)	0	
Pt2	1		0	0.20433(1)	1/4	97(1)
		sin	−0.00671(19)	0	0	
		cos	0	−0.00259(3)	0	
Ge1	1		1/2	0.24984(5)	1/4	94(3)
		sin	0.0061(5)	0	0	
		cos	0	−0.00197(9)	0	
Ge2	0.5		0	0.11020(6)	1/4	146(4)
		sin	0.0003(5)	0	0	
		cos	0	−0.00203(10)	0	
Ge3	1		0.2039(3)	0.46437(6)	1/4	120(4)
	$x4_0$ = 0.6	crenel	—	—	—	

The positional modulation can be easily understood since the orientation of the five membered rings influences the surrounding atoms of the remaining framework. The Pt1 atoms are the nearest neighbors of the five-membered rings, Ge2 is a part of the ring itself; therefore these atoms exhibit the strongest positional modulations along [100]. The remaining atoms follow the deformation of the framework, resulting in slightly lower amplitudes of the sin and cos functions (Table 3). In order to describe the crystal structure of $Ce_3Pt_4Ge_6$ a commensurate description can be used, which is obtained *via* a doubling of the *a* axis followed by a standardization. The detailed group–subgroup relations will be discussed in the following paragraph (*vide infra*). The resulting orthorhombic 3D-approximant (*Pnma*, *a* = 2618.26(14), *b* = 441.33(2) and *c* = 882.34(2) pm) describes the crystal structure without the need of half-occupied sites.

The crystallographic sites present in the modulated description split, resulting in three Ce, four Pt and six Ge sites. The structural elements described before are found as well in this model and are combined as shown in Fig. 3. In Fig. 4 the coordination polyhedra surrounding the Ce1/2 (left) and Ce3 (right) atoms are depicted. The refined anisotropic displacement parameters are listed in Table 4, interatomic distances in Table 5.

The annealing temperature and the cooling rate are important parameters for the growth of high quality crystals. The structural details of $Ce_3Pt_4Ge_6$ are comparable to the recently reported stannide $Ce_3Pt_4Sn_6$.[38] The stannide crystals showed smeared out reflections and disorder.

Group–subgroup relations

As mentioned before, the crystal structure of $Ce_3Pt_4Ge_6$ can be derived from the published orthorhombic cell with space group *Cmcm*.[11] The title compound, however, clearly shows additional reflections which were interpreted as satellite reflections, pointing towards an also *C*-centered orthorhombic

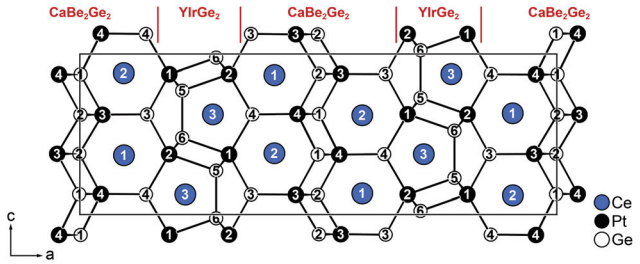

Fig. 3 Extended unit cell of the commensurate supercell structure (*Pnma*, a = 2618.26(14), b = 441.33(2) and c = 882.34(2) pm) of $Ce_3Pt_4Ge_6$. The $YIrGe_2$ and $CaBe_2Ge_2$ type parts are labelled. Ce atoms are depicted as blue, Pt atoms as black and Ge atoms as open white circles.

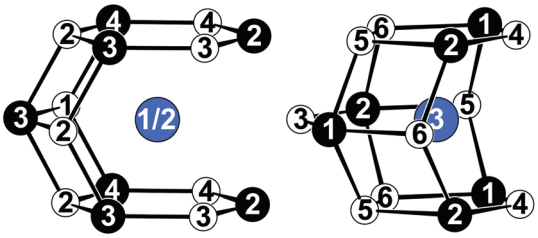

Fig. 4 Coordination environments surrounding the Ce1/2 (left) and Ce3 (right) atoms in the crystal structure of $Ce_3Pt_4Ge_6$. Ce atoms are depicted as blue, Pt atoms as black and Ge atoms as open white circles.

Table 4 Anisotropic displacement parameters (pm^2) for $Ce_3Pt_4Ge_6$, superspace group *Cmcm*(α,0,0)0s0 with α = 1/2 a^*. $U_{13} = U_{23} = 0$

Atom	U_{11}	U_{22}	U_{33}	U_{12}
Ce1	101(3)	93(3)	94(3)	0
Ce2	89(4)	98(4)	96(5)	0
Pt1	66(2)	93(2)	73(2)	0
Pt2	87(2)	109(2)	94(2)	0
Ge1	79(5)	122(6)	81(6)	0
Ge2	80(5)	96(6)	262(8)	0
Ge3	116(6)	147(6)	97(7)	−28(5)

(3 + 1)D superspace group. The according superspace group associated to the 3D space group is shown on the top left in Fig. 5. Due to α = 0.5 of the q-vector, the structure can be described as commensurately modulated. Therefore a description as approximant by a projection onto 3D space can be used. The corresponding 3D space group for this description is *Pbnm*. This is achieved by a transition of index $a4$ where a is introduced synonymously for approximant.[39]

Here two transitions are involved, a doubling of the a axis along with a loss of the centering and an origin shift of (1/4, 1/4, 0). The $a4$ transition is paralleled by two $k2$ transitions in 3D space. First a symmetry reduction from *Cmcm* to *Pbcm* by a *klassengleiche* transition of index 2 takes place, which is accompanied by an origin shift of (1/4, 1/4, 0). In the second step again a *klassengleiche* transition of index 2 takes place, allowing the doubling of the a axis. The final step is used to reach the standard setting of *Pbnm*, the orthorhombic space group *Pnma*. The group–supgroup scheme in the Bärnighausen formalism[40–43] is shown in Fig. 5. The observed disorder and diffuse superstructure reflections of[38] have their origin most likely in the occurrence of anti phase boundaries triggered by the *klassengleiche* transitions.

Magnetic properties

The magnetic properties of $Ce_3Pt_4Ge_6$ were determined *via* susceptibility and magnetization experiments. Fig. 6 (top) shows the temperature dependence of the magnetic and inverse magnetic susceptibility (χ and χ^{-1} data) measured at 10 kOe. A fit of the χ^{-1} data in the region above 50 K using the Curie–Weiss law, revealed an effective magnetic moment of μ_{eff} = 2.48(1)μ_B/Ce atom and a Weiss constant of θ_p = −39(5) K. The effective magnetic moment matches well with the theoretical value of 2.54μ_B for a free Ce^{3+}-ion indicating a stable trivalent ground state. The obvious negative value of the Weiss constant can be attributed to antiferromagnetic interactions in the paramagnetic regime, however crystal electric field splitting is a common feature in cerium intermetallics[44–46] and also responsible for the curvatures in the low temperature region.

To obtain more information about the magnetic ground state, a low-field measurement was performed in a zero-field- and field-cooled mode (ZFC/FC) which is shown in the middle graph of Fig. 6. No anomaly indicating clear magnetic ordering could be detected in this measurement, however in the low temperature region saturation effects can be observed, while the derivative dχ/dT shows a double feature at 2.5(1) K and 3.0(1) K (Fig. 6, inset). No bifurcation between the ZFC and FC curve is visible.

The bottom graph in Fig. 6 displays the magnetization isotherms of $Ce_3Pt_4Ge_6$ measured at 3, 10, and 50 K. The isotherms at 10 and 50 K both display a linear field dependency of the magnetization as expected for a paramagnetic material. With respect to the 10 K isotherm less saturation effects are visible at 50 K. At 3 K a curvature of the magnetization isotherm can be observed with weak saturation effects towards higher fields. The magnetic moment at 3 K and 80 kOe is 0.61(5)μ_B/Ce atom which is significantly below the expected saturation magnetization of 2.14μ_B/Ce according to $g_J \times J$. Magnetic susceptibility measurements reported in the literature[1] found no ordering phenomena and a reduced magnetic moment of μ_{eff} = 2.19μ_B between 40 and 140 K and a moment of μ_{eff} = 1.86μ_B above 150 K. Between 140 and 150 K an anomaly is observed which is in agreement with their resistivity measurements (*vide supra*). A magnetization isotherm at 5.5 K shows a small hysteresis. Both, the reduced moment and the anomaly between 140–150 K, are in contrast to our investigations. However the authors report their sample to be "predominantly single phase", which might be an explanation for the missing features in our investigations.

Heat capacity

In order to check for magnetic phase transitions by a second method, heat capacity measurements were conducted in the temperature region between 1.9 and 300 K. Fig. 7 (top) depicts

Table 5 Interatomic distances of the 3D supercell of $Ce_3Pt_4Ge_6$ (*Pnma*)

Ce1	2	Ge4	251.66(1)	Ce2	2	Pt3	249.77(1)	Ce3	2	Pt2	237.84(1)	Pt1	1	Ce3	239.61(1)	Pt2	2	Ce3	237.84(1)
	2	Pt4	254.45(1)		2	Ge3	255.40(1)		1	Pt1	239.61(1)		1	Ge3	251.14(1)		2	Ge6	248.77(1)
	1	Ge1	325.20(1)		1	Ge1	327.63(1)		2	Ge5	307.05(1)		1	Ge4	255.34(1)		1	Ge3	251.13(1)
	1	Ge2	327.05(1)		1	Ge2	329.60(1)		1	Ge5	311.04(1)		2	Ge5	265.86(1)		1	Ge4	255.33(1)
	1	Ge6	343.50(2)		1	Ge5	333.86(2)		2	Ge3	375.68(1)		1	Ge6	272.66(1)		1	Ge5	288.73(1)
	1	Pt3	365.87(2)		1	Pt4	356.18(2)		2	Ge4	379.92(1)		2	Pt2	395.62(2)		2	Ge5	387.29(1)
	2	Ge2	394.54(1)		2	Ge2	392.41(1)										2	Pt1	395.62(2)
	2	Ge1	396.19(1)		2	Ge1	393.96(1)										2	Ce2	395.99(1)
	2	Pt2	396.25(1)		2	Pt2	395.99(1)										2	Ce1	396.25(1)
Pt3	1	Ge3	245.44(1)	Pt4	1	Ge4	247.52(1)	Ge1	2	Ge2	220.70(1)	Ge2	2	Ge1	220.70(1)	Ge3	1	Pt3	245.44(1)
	2	Ce2	249.77(1)		1	Ge2	249.99(1)		1	Pt4	250.38(1)		1	Pt4	249.99(1)		1	Pt2	251.13(1)
	1	Ge2	251.38(1)		1	Ge1	250.38(1)		1	Pt3	251.43(1)		1	Pt3	251.38(1)		1	Pt1	251.14(1)
	1	Ge1	251.43(1)		2	Ce1	254.45(1)		1	Ce1	325.20(1)		1	Ce1	327.05(1)		2	Ce2	255.40(1)
	2	Pt4	325.42(1)		2	Pt3	325.42(1)		1	Ce2	327.63(1)		1	Ce2	329.60(1)		2	Ge5	305.67(1)
	2	Ge1	337.29(1)		2	Ge1	331.25(1)		2	Pt4	331.25(1)		2	Pt4	331.48(1)		2	Ce3	375.68(1)
	2	Ge2	337.35(1)		2	Ge2	331.48(1)		2	Pt3	337.29(1)		2	Pt3	337.35(1)		1	Ge5	388.62(2)
	1	Ce1	365.87(2)		1	Ce2	356.18(2)		2	Ce2	393.96(1)		2	Ce2	392.41(1)				
									2	Ce1	396.19(1)		2	Ce1	394.54(1)				
Ge4	1	Pt4	247.52(1)	Ge5	2	Pt1	265.86(1)	Ge6	2	Pt2	248.77(1)								
	2	Ce1	251.66(1)		1	Pt2	288.73(1)		1	Pt1	272.66(1)								
	1	Pt2	255.33(1)		2	Ge3	305.67(1)		2	Ge4	324.63(1)								
	1	Pt1	255.34(1)		2	Ce3	307.05(1)		1	Ce1	343.50(2)								
	2	Ge6	324.63(1)		1	Ce3	311.04(1)		2	Ge5	363.54(1)								
	2	Ce3	379.92(1)		1	Ce2	333.86(2)		2	Ge6	389.56(1)								
					2	Ge5	340.39(1)												
					2	Ge6	363.54(1)												
					2	Pt2	387.29(1)												
					1	Ge3	388.62(2)												

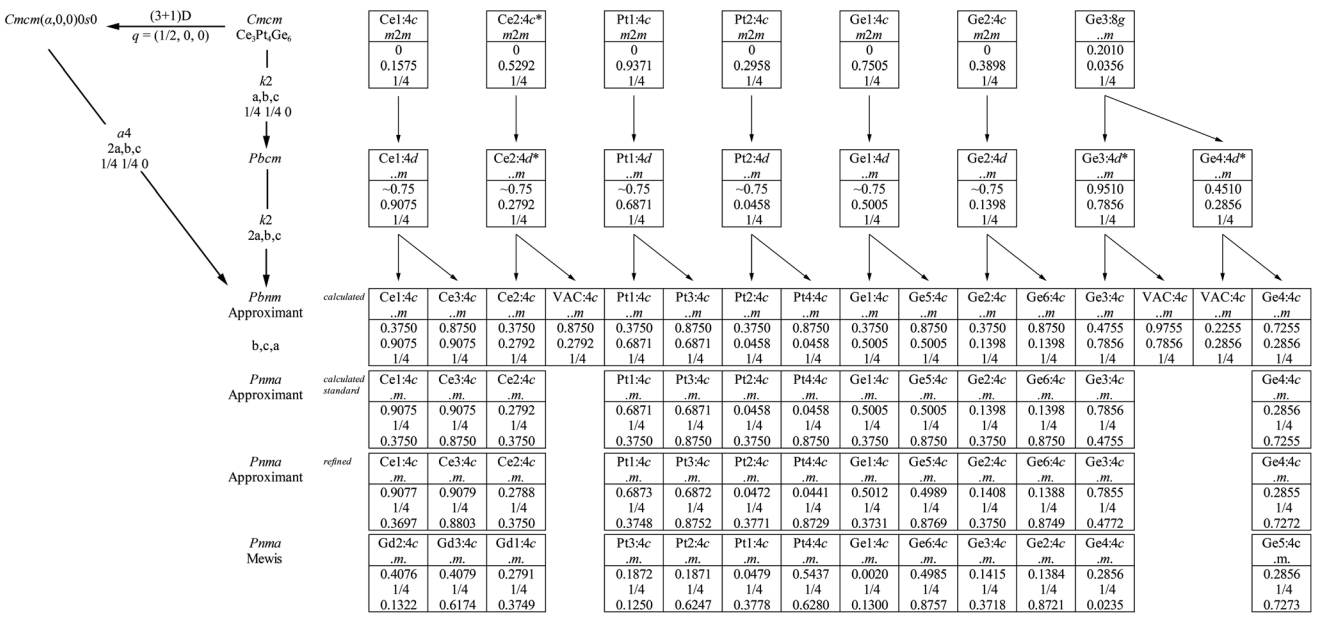

Fig. 5 Relation of the (3 + 1)D and 3D space groups of the modulated structure of $Ce_3Pt_4Ge_6$. Group–supgroup scheme in the Bärnighausen formalism[40–43] for the subcell of $Ce_3Pt_4Ge_6$ (*occupancy parameter listed as 50% in the literature[24]) and the supercell. The indices for the *klassengleiche* (*k*) symmetry reduction as well as the evolution of the atomic parameters are given. The index *a* is introduced for the formation of the approximant of the modulated structure.[39] The last line gives the atomic coordinates for $Gd_3Pt_4Ge_6$, published by Mewis in space group *Pnma*.[25]

the full temperature scale, the inset displays the low temperature region between 1.9 and 15 K. Here a clear λ-shaped anomaly can be observed with a maximum at T = 2.1(1) K indicating a magnetic phase transition. This anomaly is in good agreement with the change of the slope of the ZFC/FC curve and its derivative.

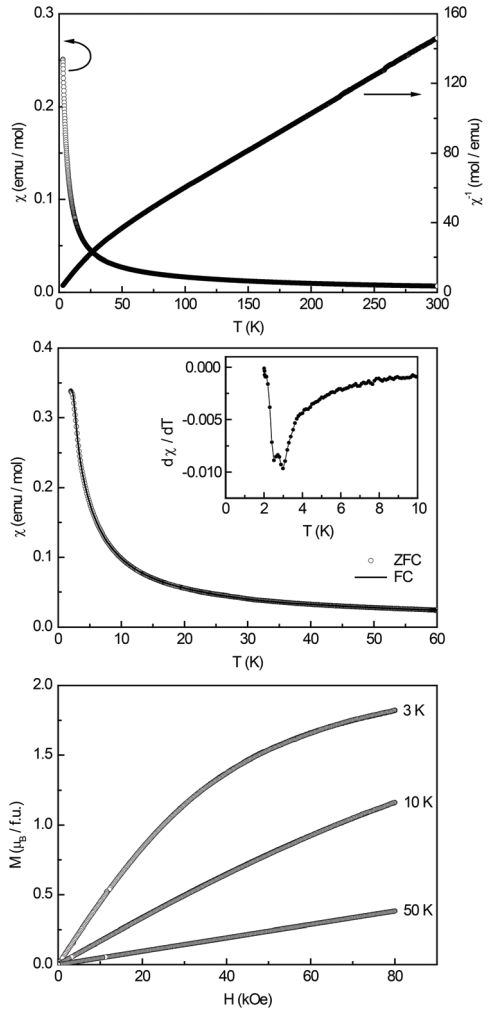

Fig. 6 Magnetic properties of $Ce_3Pt_4Ge_6$: (top) Temperature dependence of the magnetic susceptibility χ and its reciprocal χ^{-1} measured with a magnetic field strength of 10 kOe; (middle) magnetic susceptibility in zero-field (ZFC) and field-cooled (FC) mode at 100 Oe; (bottom) magnetization isotherms at 3, 10, and 50 K.

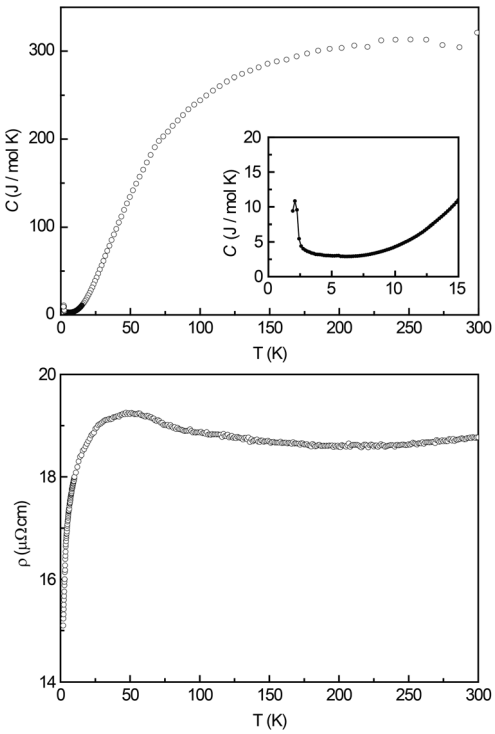

Fig. 7 Physical properties of $Ce_3Pt_4Ge_6$: (top) Heat capacity measurement in the temperature range of 1.9–300 K, the inset shows the low temperature region between 1.9–15 K, indicating a λ-shaped anomaly; (bottom) temperature dependent electrical resistivity ρ.

Electrical resistivity

Fig. 7 (bottom) shows the electrical resistivity of $Ce_3Pt_4Ge_6$ between 2 K and 300 K. Down to about 75 K, the resistivity shows a nearly temperature independent behaviour. However a shallow minimum around 200 K is clearly visible. Below 75 K, the resistivity increases with a broad maximum centred at 50 K. When going to lower temperatures, a significant drop is observed. This behaviour is indicative of Kondo lattice systems. The upturn in the resistivity can be explained by the screening of the conduction electrons at the localized $4f^1$ electron from the Ce^{3+} ions.

Conclusions

We have resynthesized $Ce_3Pt_4Ge_6$ and reinvestigated its crystal structure. A commensurate modulated structure has been found. The structure can be solved and refined in the orthorhombic superspace group $Cmcm(\alpha,0,0)0s0$ with $\alpha = 1/2\ a^*$. The superspace group correlates with the orthorhombic description of $Pr_3Pt_4Ge_6$ with space group *Pnma*, however the latter exhibits non space group specific extinction conditions. Magnetic investigations indicate that the cerium atoms are in the +3 oxidation state. Heat capacity measurements show a λ-anomaly at $T = 2.1(1)$ K. Resistivity measurements confirmed the metallic nature, the temperature dependent behavior exhibits a broad maximum centered around 50 K followed by an abrupt drop below, suggesting Kondo behavior for the title compound.

Acknowledgements

This work was supported by the Deutsche Forschungsgemeinschaft. O. N. is indebted to the NRW Forschungsschule Molecules and Materials – A common Design Principle for a PhD stipend.

Notes and references

1 A. V. Gribanov, Y. D. Seropegin, O. I. Bodak, V. N. Nikiforov, A. A. Velikhovskii and J. Mirkovic, *J. Phase Equilib.*, 1996, **17**, 196–207.

2 D. Rossi, R. Marazza and R. Ferro, *J. Less-Common Met.*, 1979, **66**, P17–P25.
3 E. Hovestreydt, N. Engel, K. Klepp, B. Chabot and E. Parthé, *J. Less-Common Met.*, 1982, **85**, 247–274.
4 A. Dommann, F. Hulliger, H. R. Ott and V. Gramlich, *J. Less-Common Met.*, 1985, **110**, 331–337.
5 M. François, G. Venturini, E. McRae, B. Malaman and B. Roques, *J. Less-Common Met.*, 1987, **128**, 249–257.
6 P. Rogl, B. Chevalier, M. J. Besnus and J. Etourneau, *J. Magn. Magn. Mater.*, 1989, **80**, 305–310.
7 G. Venturini, B. Malaman and B. Roques, *J. Less-Common Met.*, 1989, **146**, 271–278.
8 O. I. Bodak, Y. D. Seropegin, O. L. Sologub, V. K. Pecharsky and A. V. Gribanov, Abstr. Eur. Crystallogr. Meet. 12th, 1989, 2–39.
9 L. Rebelsky, K. Reilly, S. Horn, H. Borges, J. D. Thompson and R. Caspary, *J. Appl. Phys.*, 1990, **67**, 5206–5208.
10 I. Das, E. V. Sampathkumaran, R. Nagarajan and R. Vijayaraghavan, *Phys. Rev. B: Condens. Matter*, 1991, **43**, 13159–13163.
11 A. V. Gribanov, O. L. Sologub, P. S. Salamakha, O. I. Bodak, Yu. D. Seropegin and V. K. Pecharsky, *J. Alloys Compd.*, 1992, **179**, L7–L11.
12 A. V. Gribanov, O. L. Sologub, P. S. Salamakha, O. I. Bodak, Yu. D. Seropegin, V. V. Pavlyuk and V. K. Pecharsky, *J. Alloys Compd.*, 1992, **189**, L11–L13.
13 A. V. Gribanov, O. L. Sologub, P. S. Salamakha, Yu. D. Seropegin and O. I. Bodak, Tez. Dokl. Sov. Kristallokhim. Koord. Soeden 6th, 1992, 172.
14 A. V. Gribanov, Yu. D. Seropegin, O. I. Bodak, V. V. Pavlyuk, L. G. Akselrud, V. N. Nikiforov and A. A. Velikhovski, *J. Alloys Compd.*, 1993, **202**, 133–136.
15 O. Sologub, K. Hiebl, P. Rogl and O. I. Bodak, *J. Alloys Compd.*, 1995, **227**, 37–39.
16 Y. D. Seropegin, A. V. Gribanov and O. I. Bodak, Abstr. 6th Int. Conf. Crystal Chem. Intermet. Compd., 1995, 93.
17 A. V. Morozkin, Yu. D. Seropegin, A. V. Gribanov and J. M. Barakatova, *J. Alloys Compd.*, 1997, **256**, 175–191.
18 D. Niepmann, R. Pöttgen, Yu. M. Prots' and W. Jeitschko, *Z. Kristallogr.*, 1998, (Suppl. 15), 49.
19 Yu. M. Prots', R. Pöttgen, D. Niepmann, M. W. Wolff and W. Jeitschko, *J. Solid State Chem.*, 1999, **142**, 400–408.
20 J. Sakurai, D. Huo, D. Kato, T. Kuwai, Y. Isikawa and K. Mori, *Physica B*, 2000, **281&282**, 98–100.
21 Z. Hossain, T. Takabatake, C. Geibel, P. Gegenwart, I. Oguro and F. Steglich, *J. Phys.: Condens. Matter*, 2001, **13**, 4535–4542.
22 W. Hermes, U. Ch. Rodewald, B. Chevalier and R. Pöttgen, *Z. Naturforsch., B: Chem. Sci.*, 2007, **62**, 613–616.
23 R. Gumeniuk, H. Borrmann, A. Ormeci, H. Rosner, W. Schnelle, M. Nicklas, Yu. Grin and A. Leithe-Jasper, *Z. Kristallogr.*, 2010, **225**, 531–543.
24 G. Venturini and B. Malaman, *J. Less-Common Met.*, 1990, **167**, 45.
25 A. Imre, A. Hellmann and A. Mewis, *Z. Anorg. Allg. Chem.*, 2006, **632**, 1145–1149.
26 A. Gribanov, P. Rogl, A. Grytsiv, Yu. Seropegin and G. Giester, *J. Alloys Compd.*, 2013, **571**, 93–97.
27 B. Heying and R. Pöttgen, unpublished results.
28 R. Pöttgen, T. Gulden and A. Simon, *GIT Labor-Fachz.*, 1999, **43**, 133–136.
29 R. Pöttgen, A. Lang, R. D. Hoffmann, B. Künnen, G. Kotzyba, R. Müllmann, B. D. Mosel and C. Rosenhahn, *Z. Kristallogr.*, 1999, **214**, 143–150.
30 K. Yvon, W. Jeitschko and E. Parthé, *J. Appl. Crystallogr.*, 1977, **10**, 73–74.
31 P. J. Becker and P. Coppens, *Acta Crystallogr., Sect. A: Cryst. Phys., Diffr., Theor. Gen. Cryst.*, 1974, **30**, 129–147.
32 L. J. van der Pauw, *Philips Res. Repts.*, 1958, **13**, 1–9.
33 L. Palatinus and G. Chapuis, *J. Appl. Crystallogr.*, 2007, **40**, 786–790.
34 V. Petříček, M. Dušek and L. Palatinus, *Jana2006. The crystallographic computing system*, Institute of Physics, Praha, Czech Republic, 2006.
35 V. Petříček, M. Dušek and L. Palatinus, *Z. Kristallogr.*, 2014, **229**, 345–352.
36 H. T. Stokes, B. J. Campbell and S. van Smaalen, *Acta Crystallogr., Sect. A: Fundam. Crystallogr.*, 2011, **67**, 45–55.
37 S. van Smaalen, B. J. Campbell and H. T. Stokes, *Acta Crystallogr., Sect. A: Fundam. Crystallogr.*, 2013, **69**, 75–90.
38 W. Paschinger, K. Yubuta, Y. Saiga, T. Takabatake, G. Giester and P. Rogl, *Solid State Sci.*, 2016, **55**, 48–57.
39 O. Niehaus, R.-D. Hoffmann, S. Tencé, B. Chevalier and R. Pöttgen, *Z. Kristallogr.*, 2015, **230**, 579–591.
40 H. Bärnighausen, *Commun. Math. Chem.*, 1980, **9**, 139–175.
41 H. Bärnighausen and U. Müller, *Symmetriebeziehungen zwischen den Raumgruppen als Hilfsmittel zur straffen Darstellung von Strukturzusammenhängen in der Kristallchemie*, Universität Karlsruhe und Universität-Gh Kassel, Germany, 1996.
42 U. Müller, *Z. Anorg. Allg. Chem.*, 2004, **630**, 1519–1537.
43 U. Müller, *Symmetry Relationships between Crystal Structures*, Oxford University Press, 2013.
44 P. Javorský, L. Havela, V. Sechovský, H. Michor and K. Jurek, *J. Alloys Compd.*, 1998, **264**, 38–42.
45 B. Chevalier and J. L. Bobet, *Intermetallics*, 2001, **9**, 835–838.
46 W. Hermes, R. Mishra, U. C. Rodewald and R. Pöttgen, *Z. Naturforsch., B: Chem. Sci.*, 2008, **63b**, 537–542.

